Published in final edited form as:
*J Magn Reson Imaging*. 2010 May ; 31(5): 1106–1116. doi:10.1002/jmri.22155.

# Quantitative 4D Transcatheter Intraarterial Perfusion MRI for Monitoring Chemoembolization of Hepatocellular Carcinoma

**Dingxin Wang, PhD**[1,2], **Brian Jin, BA**[1], **Robert J. Lewandowski, MD**[1], **Robert K. Ryu, MD**[1], **Kent T. Sato, MD**[1], **Mary F. Mulcahy, MD**[3,5], **Laura M. Kulik, MD**[4], **Frank H. Miller, MD**[1], **Riad Salem, MD, MBA**[1,3,5], **Debiao Li, PhD**[1,2], **Reed A. Omary, MD, MS**[1,2,5], and **Andrew C. Larson, PhD**[1,2,5,*]

[1] Department of Radiology, Northwestern University, Chicago, Illinois, USA

[2] Department of Biomedical Engineering, Northwestern University, Chicago, Illinois, USA

[3] Department of Medicine, Northwestern University, Chicago, Illinois, USA

[4] Department of Hepatology , Northwestern University, Chicago, Illinois, USA

[5] Feinberg School of Medicine, and Robert H. Lurie Comprehensive Cancer Center, Northwestern University, Chicago, Illinois, USA

## Abstract

**Purpose—**To develop a fully quantitative 4D transcatheter intraarterial perfusion (TRIP) MRI technique and prospectively test the hypothesis that quantitative 4D TRIP-MRI can be used clinically to monitor intra-procedural liver tumor perfusion reductions during transcatheter arterial chemoembolization (TACE).

**Materials and Methods—**TACE was performed within an x-ray DSA-MRI procedure suite in 16 patients with hepatocellular carcinoma. Quantitative 4D TRIP-MRI with targeted radiofrequency field mapping and dynamic longitudinal relaxation rate mapping was used to monitor changes in tumor perfusion during TACE. First-pass perfusion analysis was performed to produce intra-procedural blood flow (Fρ) maps. Mean liver tumor perfusions before and after TACE were compared with a paired t-test ($\alpha = 0.05$).

**Results—**Perfusion reductions were successfully measured with quantitative 4D TRIP-MRI in 22 separate tumors during 18 treatment sessions. Mean tumor perfusion Fρ decreased from 16.3 (95% CI: 10.7–21.9) before TACE to 5.0 (95% CI: 3.5–6.5) (mL/min/100mL) after TACE. Tumor perfusion reductions were statistically significant ($P < 0.0005$), with a mean absolute perfusion change of 11.4 (95% CI: 5.6–17.1) (mL/min/100mL) and a mean percentage reduction of 61.0% (95% CI: 48.3%–73.6%).

**Conclusions—**Quantitative 4D TRIP-MRI can be successfully performed within clinical interventional settings to monitor intra-procedural changes in liver tumor perfusion during TACE.

### Keywords

TRIP-MRI; perfusion; quantitative imaging; TACE; hepatocellular carcinoma; liver tumor

[*]Corresponding author: Andrew C. Larson, Ph.D., Northwestern University, Department of Radiology, 737 N. Michigan Avenue, Suite 1600, Chicago, IL 60611, Tel: (312) 926-3499 Fax: (312)926-5991, a-larson@northwestern.edu.

## INTRODUCTION

Hepatocellular carcinoma (HCC) is the fifth most common malignancy (1) and the fourth leading cause of cancer death worldwide (2), with an increasing incidence over the last 15–20 years (3). Transcatheter arterial chemoembolization (TACE) is a widely accepted therapy for treatment of unresectable HCC that are not amenable to surgery. Randomized controlled trials have demonstrated an improved patient survival benefit with TACE versus best supportive care (4,5). However, the relationship between TACE-induced tumor perfusion changes and therapeutic outcome remains unknown. There is no consensus to support which TACE embolic endpoint—stasis (ie, complete blockage of antegrade blood flow to tumor) or substasis (ie, partial reduction of forward blood flow to tumor)—is preferable. While under-embolization may undermine therapeutic efficacy, over-embolization (ie, embolization to a level beyond any therapeutic benefit) or repeated embolizations may lead to arterial occlusion, accelerated liver decompensation and failure (6,7), and potential induction of cancer angiogenesis and tumor recurrence (8,9). Although a four-point subjective angiographic chemoembolization endpoint (SACE) scale (10) was developed to classify TACE embolic endpoints, objectively quantifying tumor perfusion remains an obstacle with x-ray digital subtraction angiography (DSA) due to its high subjectivity and variability in angiographic endpoint monitoring (10).

With the increasing availability of combined x-ray DSA-MRI procedure suites, it is now possible to use DSA to guide catheter placement and use MRI to monitor intra-procedural functional therapeutic effects (11,12). **TR**anscatheter **I**ntraarterial **P**erfusion (TRIP) MRI is an intra-procedural perfusion measurement technique that employs catheter-directed intraarterial injections of contrast material (13). This technique can be used to objectively monitor changes in tumor perfusion during liver-directed embolotherapies (12,14) and verify the distribution of injected chemoembolic material before delivery (15). Semi-quantitative TRIP-MRI was initially developed and evaluated in preclinical rabbit intra-hepatic tumor embolization studies (14,16), and its early clinical translation was demonstrated in liver cancer patients undergoing chemoembolization in a combined clinical x-ray DSA-MRI suite (12,17). A quantitative four-dimensional (4D) TRIP-MRI technique (serial iterative three-dimensional (3D) volumetric perfusion imaging) including rigorous radiofrequency field ($B_1$) calibration, dynamic tissue longitudinal relaxation rate ($R_1$) measurements, and a peak gradient method for blood flow analysis was recently developed and validated during preclinical animal model studies (18). An additional refinement now includes the use of quantitative first-pass perfusion analysis methods with more sophisticated pharmacokinetic modeling approaches tailored for TRIP-MRI datasets. The purpose of our study was to develop a fully quantitative 4D TRIP-MRI acquisition and analysis approach and prospectively test the hypothesis that quantitative 4D TRIP-MRI can be used clinically to monitor intra-procedural liver tumor perfusion reductions during TACE procedures in patients with HCC.

## MATERIALS AND METHODS

### Clinical Setting and Patients

This prospective study was compliant with Health Insurance Portability and Accountability Act, and was approved by our local Institutional Review Board. We obtained informed consent from all patients.

From September 2008 through September 2009, we prospectively enrolled 16 consecutive patients with surgically unresectable HCC presenting for x-ray DSA-MRI monitored TACE at a university-affiliated hospital in a large metropolitan area. All patients were deemed candidates for TACE at a weekly institutional multi-disciplinary hepatic oncology conference. We used a modified set of inclusion and exclusion criteria by Brown et al (19). We enrolled patients who a) were older than 18 years; b) had an Eastern Cooperative Oncology Group

(ECOG) performance score no greater than 2; c) had Child-Pugh class A or B; d) had focal or multi-focal malignancy; e) had no contraindications to MRI scan; and f) provided informed consent. We excluded patients who had: a) a life expectancy of less than 6 months; b) an ECOG performance score no smaller than 3; c) Child-Pugh class C; d) uncorrectable coagulopathy (i.e. International Normalized Ratio > 1.5); e) a total bilirubin level grater than 4.0 mg/dL; f) a serum creatininelevel grater than 2.0 mg/dL; g) uncorrectable thrombocytopenia (platelet count < 50,000/μL); or h) contraindications to MRI, such as pacemaker or cochlear implant. Patients with portal vein thrombosis were included if super-selective segmental TACE was technically feasible (20). Patients were excluded if they did not undergo intra-procedural MRI examination during TACE. Detailed patient and tumor characteristics and HCC staging of enrolled patients are listed in Tables 1–2.

The diagnosis of HCC was established with biopsy and/or non-invasively based on the presence of a tumor with greater than 2 cm diameter plus characteristic imaging findings in the setting of cirrhosis (21), or a serum α-fetoprotein level of no less than 400 ng/mL (22). Patients were deemed to be ineligible for surgical HCC resection for the following reasons: a) concurrent comorbidities including cardiac or respiratory compromise, b) recurrent or multi-lobar disease, c) cirrhosis or portal hypertension, d) vascular invasion, e) high tumor burden (> 25% of the total liver volume), and/or f) contraindications to general anesthesia. Two attending transplant surgeons present at the institutional weekly multidisciplinary HCC conference accessed surgical unresectability.

## X-ray DSA-MRI Procedure Suite

We performed all TACE procedures using a dedicated x-ray DSA-MRI procedure suite (Miyabi, Siemens, Erlangen, Germany). This system integrated a flat panel x-ray DSA Artis–dTA unit with a 1.5T Espree wide-bore MR unit via a moving interventional radiology (IR) procedure table. Patients, with their positions registered to the moving table, were transferred between the DSA and MRI units according to our institution's safe transfer protocol.

## TACE

All TACE procedures were performed by one of four board-certified attending interventional radiologists who specialize in interventional oncology. Patients were prepared and draped in sterile fashion in the supine position on the IR procedure table. Through arterial access via the right common femoral artery, we inserted a 5-F visceral catheter (typically either Simmons or cobra shapes) and performed initial mapping visceral x-ray DSA. Under subsequent radiographic angiography guidance, a 2.8-F microcatheter (Renegade Hi-Flow, Boston Scientific, Natick, Mass) was advanced coaxially over a 0.016-inch-diameter guide wire (Headliner, Terumo, Tokyo, Japan) to super-select either the hepatic lobar or segmental hepatic artery supplying the targeted tumor. X-ray DSA was performed by using iohexol injection (Omnipaque 350, Amersham Health, Princeton, New Jersey).

After the attending interventional radiologist selected the appropriate catheter position for TACE, patients were transferred to the adjacent MRI unit on the moving IR procedure table. Vascular catheter systems were covered with a sterile drape so that the MR array abdominal coil could be placed. We performed baseline MRI prior to TACE administration and then transferred patients back to the x-ray DSA suite for TACE. A 1:1 solution of emulsifying contrast medium and chemotherapy was prepared by mixing 10 mL of ethiodized oil (Ethiodol; Savage Laboratories, Melville, New York) with a 10 mL mixture of three-drug chemotherapy consisting of 100 mg of cisplatin, 30 mg of doxorubicin, and 30 mg of mitomycin C. Under direct fluoroscopic monitoring, we infused this solution in 1–3-mL aliquots, typically until there was some slowing of antegrade blood flow to the targeted tumor. We then completed TACE by injecting 500–700 μm diameter trisacryl gelatin microspheres (Embosphere;

Biosphere Medical, Rockland, Mass) mixed with iohexol. The amount of injected chemoembolic material and angiographic endpoint were determined at the discretion of the attending interventional radiologist according to the SACE scale (10). In general, we employed a substasis embolic endpoint in patients with increased bilirubin levels and/or high likelihood to undergo repeated TACE, whereas a stasis endpoint in patients with normal bilirubin levels and/or low likelihood to be re-treated in the same targeted artery. After TACE, patients were transferred to the adjacent MRI unit for post-TACE imaging. After this completion MR imaging examination, we transferred patients back to the x-ray DSA suite, removed the vascular sheath, and achieved groin hemostasis with manual compression. Immediately after completion of TACE, non-contrast enhanced computed tomography (CT) was performed to assess the distribution of the chemotherapy emulsifying contrast agent.

## MR Imaging

After being transferred into the magnet bore, patients underwent intra-procedural MRI in the supine position. A 2-channel anterior array abdominal coil and a 6-channel posterior array coil were used for signal acquisition. MR images were acquired during multiple breath-holds at expiration. We first acquired multi-slice axial and coronal two-dimensional (2D) turbo-spin-echo (TSE) T2-weighted and axial spoiled gradient-recall-echo (GRE) T1-weighted images covering the entire liver to locate optimal imaging positions for subsequent 4D TRIP-MRI. Prior to each TRIP-MRI dynamic scan, we acquired baseline 3D $R_1$ maps in transverse orientations, providing full spatial coverage of the targeted liver segment(s). The baseline 3D $R_1$ mapping was performed using a 3D variable flip angle (VFA) GRE method (18) with the following parameters: TR/TE = 4.0/1.72 msec, flip angle (FA) = 2°, 9°, 15°, 19°, 3 averages, 192×108×24–192×132×24 matrix, 400–450 mm field of view (FOV), 5 mm interpolated partition thickness, 670 Hz/pixel bandwidth, 6/8 partial Fourier in both the slice and phase encoding directions, 33% slice over sampling, generalized autocalibrating partially parallel acquisition factor, two. To calibrate $B_1$ inhomogenity for quantitative perfusion imaging in the TACE targeted region, we measured *in vivo* targeted 3D $B_1$ maps in transverse orientations using TSE based 3D reduced FOV catalyzed double-angle method (DAM) (23,24) with the following parameters: TR/TE = 400/12 msec, excitation/compensation FA = 60°/120° and 120°/60°, refocusing FA = 180°, catalyzation chain pulse FA = 90°, 3 catalyzation chain pulses, 660 Hz/pixel bandwidth, echo train length = 7, 6/8 partial Fourier in both the slice and phase encoding directions, 50% slice oversampling, 128×28×16 matrix. Flow saturation bands were applied on both sides of the $B_1$ imaging slab in the slice direction to minimize inflow effects. This targeted 3D $B_1$ mapping technique allowed time-efficient TSE image acquisition within a single breath-hold, and provided sufficient spatial coverage for local $B_1$ calibration in the selected targeted HCC and surrounding treatment regions. Multiple targeted 3D $B_1$ maps of different regions were acquired to increase spatial coverage if deemed necessary. 4D TRIP-MRI was then performed using a 3D GRE sequence with identical parameters to the VFA method at 15° FA for rapid dynamic $R_1$ mapping with the targeted 3D imaging volume consecutively acquired 15 times at 2.1-second sampling rate.

Five seconds after the beginning of the dynamic image acquisition, the interventional radiologist manually injected 5.0 mL 20% gadopentetate dimeglumine solution (Gd-DTPA, Magnevist, Berlex, Wayne, New Jersey) at a rate of 1 mL/sec through the existing hepatic artery catheter. Our injection protocol was empirically designed, based on the targeted vessel caliber and blood flow rates, as well as the targeted volume, to demonstrate perfusion to the targeted liver segment(s), while avoiding reflux of injected contrast agent into non-targeted angiographic territories. Our injection protocol was also developed to be consistently applicable for all the patients before and after TACE in this study, and to achieve adequate dynamic signal enhancement in the targeted liver segment(s) while avoiding signal saturation.

After each 4D TRIP-MRI dynamic scan, we acquired multi-slice 2D T1-weighted contrast-enhanced (CE) GRE images of the liver in the axial orientation.

## MR Data Analysis

Each TRIP-MRI dataset was exported and processed off-line with Matlab software package (Mathworks, Natick, Mass).

**$B_1$ Calibrated Dynamic $R_1$ mapping and Contrast Agent Concentration Calculation—**A flip angle correction factor map ($C_{FA}$) was first calculated using the ratio between two catalyzed DAM images at 120° and 60° FAs (23):

$$C_{FA}(r)=\arccos(SI_{120}(r)/2SI_{60}(r))/60 \quad [1]$$

The transverse matrix size of the $C_{FA}$ map was scaled 1.5 times with bilinear interpolation to 192×42 to match the resolution of the $R_1$ measurement. The nominal excitation FA ($\alpha_{nom}$) was then corrected to actual FA value ($\alpha$): $\alpha(r) = \alpha_{nom} \times C_{FA}(r)$ in subsequent calculations.

Voxel-wise $B_1$ calibrated VFA (2°, 9°, 15°, and 19°) spoiled GRE steady-state signal intensities were transformed and fitted to a linear curve to generate the baseline 3D $R_1$ map:

$$\frac{SI(r,\alpha_i)}{\sin(C_{FA}(r)\alpha_i)}=\exp(-TR\times R_1(r))\frac{SI(r,\alpha_i)}{\tan(C_{FA}(r)\alpha_i)}+M_0(r)(1-\exp(-TR\times R_1(r))) \quad [2]$$

where $M_0(r)$ is a constant associated with equilibrium magnetization and receiver coil gain.

The $B_1$ calibrated 15° FA dynamic TRIP-MR images were then translated into a time series of 3D $R_1(t)$ maps (18) (neglecting the $T_2^*$ effect with short TE):

$$R_1(r,t))=-\frac{1}{TR}\ln\left(\frac{1-\frac{SI_d(r,t,\alpha_{15})}{SI(r,\alpha_{15})}\frac{(1-\exp(-TR\times R_{10}(r)))}{(1-\exp(-TR\times R_{10}(r))\cos(C_{FA}(r)\alpha_{15}))}}{1-\cos(C_{FA}(r)\alpha_{15})\frac{SI_d(r,t,\alpha_{15})}{SI(r,\alpha_{15})}\frac{(1-\exp(-TR\times R_{10}(r)))}{(1-\exp(-TR\times R_{10}(r))\cos(C_{FA}(r)\alpha_{15}))}}\right) \quad [3]$$

The difference between baseline $R_1$ ($R_{10}$) and $R_1(t)$ maps were converted into the 4D tissue contrast agent concentration $C_t(t)$ maps using the classic relationship:

$$C_t(t)=\frac{[R_1(t)-R_{10}]}{\Re_1} \quad [4]$$

where $\Re_1$ is the longitudinal relaxivity of Gd-DTPA ($3.9 Ls^{-1}mmol^{-1}$ at 37°C) (25). This conversion assumes fast exchange of water protons between compartments and relatively uniform Gd-DTPA relaxivity inside blood as well as the extra-vascular space of the liver (26,27). These 4D $C_t(t)$ maps were then used for quantitative perfusion analysis.

**Quantitative First-Pass Perfusion Analysis—**For first-pass perfusion analyses, targeted intra-hepatic arterial injection of the contrast agent simplifies pharmacokinetic modeling within the liver; specifically, one needs only consider a single input model rather than a complex dual-input (portal and arterial) model (14,18). According to the distributed parameter (DP) model (28) and the adiabatic approximation to the tissue homogeneity (AATH) model

(29), we can describe contrast tracer uptake in the liver during the microvascular transit phase of the contrast bolus (i.e. before any venous drain) as:

$$C_t(t)=F_\rho(1-Hct)\int_0^t C_p(t-\tau)d\tau \quad (0<t<T_c) \qquad [5]$$

where $C_t(t)$ is the time series of contrast agent concentration in the liver tissue (mmol/mL), $C_p(t)$ is the time series of contrast concentration in the arterial blood plasma (mmol/mL), also known as the arterial input function (AIF), *Hct* is hematocrit (assumed to be 0.45 (30), F is the hepatic arterial blood flow (mL/min/100g), ρ is the tissue density of liver tissue (100g/mL), and $T_c$ is the mean transit time (sec). Based upon typical literature mean transit times for the human liver (12.7–51 seconds depending on pathological conditions) (28,31,32) and visual inspection of the curvature of measured $C_t(t)$ from both current and prior clinical TRIP-MRI studies (12,17), we chose to include data points acquired within only the first 12–15 seconds after contrast bolus arrival during a period anticipated to be representative of the microvascular transit phase. Thus, our first-pass modeling approach utilizes only the microvascular transit phase of contrast tracer kinetics ($0 < t < T_c$) (28), during which the total amount of injected contrast media should remain inside the imaged tissue volume before exiting through venous outflow. This simplified approach avoids the curve fitting complexity associated with DP and AATH models (28,29), and at the same time allows dedicated measurement of blood perfusion, which is mixed with capillary permeability in the commonly used Tofts model (30). However, just as with DP and AATH models, this simplified approach does not recognize the difference and exchange of contrast tracer between vascular and interstitial spaces during the microvascular transit phase.

Furthermore, super-selective catheter-directed delivery of contrast agent should permit first-pass perfusion analysis without direct measurement of $C_p(t)$ within the relatively small hepatic arteries distal to the catheter-tip. Given that the super-selective transcatheter bolus injection should temporarily suppress antegrade blood flow and control the maximum vascular contrast agent concentration at the catheter tip immediately proximal to the tumor tissues (18), we can estimate AIF, i.e. $C_p(t)$, using prior information about the bolus injection parameters. Suggested by the waveform of previously measured AIF during a TRIP-MRI study (14) and ignoring dispersion effects, we approximated $C_p(t)$ as a normalized convolution of the normalized catheter input function, $C_c(t)$, and an exponential deformation function, $\exp(-\beta t)$, scaled by the injected contrast agent concentration, $C_{inject}$:

$$C_p(t)=C_{inject}\frac{\int_0^t C_c(\tau)\exp(-\beta(t-\tau))d\tau}{\max\left(\int_0^t C_c(\tau)\exp(-\beta(t-\tau))d\tau\right)} \qquad [6]$$

where $C_c(t)=\begin{cases}0 & t<T_{start}\,\|\,t>T_{end}\\ 1 & T_{start}\le t\le T_{end}\end{cases}$ is a normalized boxcar function, with 0 meaning no contrast solution being injected, 1 meaning contrast solution being injected, and $T_{start}$ and $T_{end}$ representing the beginning and ending times for the transcatheter injection of contrast solution. $T_{end}-T_{start}$ = 5 seconds for our current study. Eq. 6 gives the restrictive first-pass AIF estimation. The deformation function$\exp(-\beta t)$ illustrates the process of how $C_p(t)$ is deformed from an ideal boxcar catheter input function $C_c(t)$ to its actual shape, with β ($s^{-1}$) being a unique local parameter. While the normalized convolution modulates the waveform of the AIF, $C_{inject}$ regulates the amplitude of the AIF. Based upon the 20% Gd solution injection, $C_{inject}$ was calculated to be 100 mmol/L for our current study.

The measured $C_t(t)$ curves were interpolated 10 times and fitted with the combined Eqs. 5 and 6 to calculate two unknown parameters: Fρ and β. During curve fitting, $C_c(t)$ was automatically aligned with $C_t(t)$ in an interpolated temporal fashion to account for different bolus arrival times within different tissue regions. As β is not a characteristic of perfusion, we used only the kinetic parameter Fρ to quantify intra-procedural HCC perfusion.

### Statistical Analysis

Statistical analyses were performed using a commercially available software package (Origin 7.0, OriginLab, Northampton, MA). On the basis of T2-weighted images, CE T1-weighted images, and TRIP-MR images, tumor regions of interest (ROI) were drawn on perfusion maps for each TACE treated tumor by consensus of two observers under the instruction of an attending interventional radiologist. We calculated the change in HCC perfusion after TACE as the absolute reduction as well as the percentage reduction from pre-TACE perfusion values. Intra-procedural HCC perfusion Fρ (mL/min/100mL), absolute perfusion change Fρ (mL/min/100mL) and perfusion reduction (%) were reported as means and 95% confidence intervals (CIs). TRIP-MRI perfusion Fρ values before TACE and after TACE for each tumor were compared using a paired two-tailed t-test. A P value of less than 0.05 was considered to indicate a significant difference.

## RESULTS

The 16 patients successfully underwent a total of 18 separate x-ray DSA-MRI monitored TACE sessions with 22 separate HCC foci treated. Quantitative 4D TRIP-MRI was successfully used to monitor intra-procedural perfusion changes in each TACE session. Typical time to complete the entire TACE procedure was 2.5 hours, with an average 10-minute transfer time between the DSA and MRI units, and a typical 20-minute imaging time for each course of intra-procedural MRI measurements.

Quantitative analyses of the 4D TRIP-MRI datasets were successfully performed in all cases. Representative fittings of the voxel-wise concentration time curves using the proposed first-pass perfusion model are shown in Fig. 1. These examples were obtained from a patient with particularly good breath-hold compliance during the 4D TRIP-MRI acquisition. The measured $C_t(t)$ curves clearly exhibited alteration in contrast uptake caused by TACE. The proposed model fitting closely corresponded to the original voxel-based $C_t(t)$ curves both before and after TACE.

Catheter positioning, arterial structure, and antegrade blood flow were seen clearly in pre-TACE iodinated contrast x-ray DSA images (Fig. 2a, Fig. 3a). Reduced antegrade blood flow and reduced or no tumor blush in the post-TACE x-ray DSA images were reflective of immediate embolic effects (Fig. 2b, Fig. 3b). Regional liver enhancement corresponding to the targeted transcatheter intraarterial Gd-DTPA contrast injection was seen in the pre-TACE peak enhanced 4D TRIP-MR images from the same patients (Fig. 2c and Fig. 3c). Reduced contrast uptake in post-TACE peak enhanced 4D TRIP-MR images implied the blockage of antegrade blood flow in agreement with angiographic findings (Fig. 2d, Fig. 3d). Quantitative intra-procedural Fρ maps clearly showed the baseline perfusion distribution before TACE and resultant perfusion alteration after TACE in the tumors within the targeted vascular territories (Fig. 2e–f, Fig. 3e–f). Intra-procedural Fρ maps together with axial T2-weighted anatomic images (Fig. 4a, b, d, e, g, h, j k) quantitatively demonstrated spatially heterogeneous TACE-induced tumor perfusion reductions. The region of perfusion reductions in the targeted tumor was qualitatively confirmed by the post-TACE abdominal CT images showing ethiodized oil contrast accumulation within these same regions (Fig. 4c, f, i, l). 4D Fρ maps co-registered to T2-weighted anatomic images provided localized intra-procedural perfusion information with volumetric coverage within the targeted treatment region (Fig. 5).

In 21 of the 22 tumors treated with TACE, we were able to draw ROIs covering the entire tumor. For the remaining tumor, with longitudinal diameter larger than our 4D TRIP-MRI sampled slab thickness, we selected ROIs containing only those tumor tissues present within the computed perfusion maps.

Mean intra-procedural Fρ values for HCC perfusion were significantly reduced from 16.3 (95% CI: 10.7–21.9) before TACE to 5.0 (95% CI: 3.5–6.5) (mL/min/100mL, $P < 0.0005$) after TACE (Fig. 6). These results corresponded to a mean absolute perfusion change of 11.4 (95% CI: 5.6–17.1) (mL/min/100mL), with range from 0.1 to 60.0 (ml/min/100mL) and a mean percentage Fρ reduction of 61.0% (95% CI: 48.3%–73.6%), with range from 1.0% to 97.9%.

## DISCUSSION

In this prospective study, we developed a fully quantitative 4D TRIP-MRI technique and translated this technique clinically using a state-of-the-art integrated x-ray DSA-MRI unit to monitor 18 separate TACE sessions for 16 HCC patients. Our results showed that fully quantitative 4D TRIP-MRI can be applied successfully to measure intra-procedural reductions in perfusion to the targeted tumor during TACE procedures. Our proposed first-pass analysis approach successfully generated intra-procedural perfusion maps which demonstrated statistically significant differences in perfusion within the targeted tumors after TACE.

Quantitative 4D TRIP-MRI offers an objective, quantitative, and effective method to monitor changes in perfusion to the targeted tumors during TACE. This objective, quantitative capacity cannot be provided with traditional subjective x-ray DSA TACE monitoring approaches. Quantification of 4D TRIP-MRI is achieved through two important steps. The first step is rigorous baseline and dynamic $R_1$ measurements for quantitative voxel-wise estimations of tracer concentration time series. The $R_1$ measurement procedure intra-procedurally calibrates the transmitted $B_1$ inhomogeneity and eliminates the influences from the receiver coil sensitivity profile. The second step involves quantitative perfusion analysis based on pharmacokinetic models describing physiologic tissue processes. In this study, we derived a parameter Fρ directly linked to blood flow in our proposed first-pass pharmacokinetic analysis. Due to these quantitative efforts, our intra-procedural perfusion maps exhibited different spatial patterns within the targeted tumor regions when compared to static CE T1-weighted images (Fig 2 and Fig 3). The signal intensity of these anatomic CE images comprised information of transmitted $B_1$, receiver coil sensitivity, static tissue contrast agent concentration, and underlying tissue characteristics other than absolute perfusion. The objective, quantifiable, and multi-dimensional functional capacity of quantitative 4D TRIP-MRI could be used to provide insights into the relationship between tumor perfusion response and therapeutic outcomes following TACE, to facilitate standardization of TACE embolic endpoints (10,12,14), to target a potential specific reduction in tumor perfusion to optimize TACE procedures. The advancement of quantitative 4D TRIP-MRI can be viewed within the context of the development of 4D image-guided interventional techniques to quantitatively validate treatment endpoints (biomarkers), which was highlighted in the Biomedical Imaging Research Opportunities Workshop IV in 2006 (33).

The newly proposed first-pass perfusion analysis approach provides several practical and technical benefits for successful clinical application of quantitative 4D TRIP-MRI. Foremost, this simplified first-pass kinetic model enables calculation of blood perfusion using data acquired within only 12–15 seconds after contrast bolus arrival (i.e. within typical mean transit time of the liver). This is in contrast to traditional dynamic contrasted enhanced (DCE) MRI analyses which assess datasets collected several minutes to an hour after contrast bolus injection. This shorter duration of data acquisition allows single breath-hold dynamic TRIP-MRI avoiding respiratory motion artifacts due to motion during longer acquisition times,

simplifying image co-registration, and shortening the requisite burden of overall imaging times during an interventional procedure. Secondly, this first-pass perfusion analysis permits robust derivation of a kinetic parameter Fρ that should solely reflect blood flow alterations during TACE. The theory of our approach was based on advanced DP and AATH models. As these models are more complex and thorough than the general Tofts model in describing contrast tracer kinetics, the blood flow (Fρ) can be quantified separately from permeability surface area product, unlike the commonly used $K^{trans}$ in the Tofts model. However, due to the complexity of DP and AATH models (with at least four unknown fitting parameters), the uniqueness of the model solution can be an issue (34). In contrast, the simplicity of the proposed TRIP-MRI first-pass perfusion model (with only two unknown fitting parameters, Fρ and β) ensures fast and robust curve fitting to achieve a unique model solution. Additionally, our first-pass perfusion analysis estimates the local AIF from model curve fitting using knowledge of the controlled contrast injection. It circumvents direct AIF measurement for TRIP-MRI, which can be difficult due to the small vessel caliber distal to the catheter tip. Finally, the first-pass kinetic analysis minimizes the impact from previous injected residual contrast agent upon blood flow calculations. With the assumption of identical diffusion forces, a low concentration of residual tissue contrast agent is expected to contribute a negligible influence on the contrast tracer uptake during the vascular transit phase ($0 < t < T_C$) (18). These practical and technical benefits should allow quantitative 4D TRIP-MRI to be applied clinically.

To the best of our knowledge, our study for the first time quantifies intra-procedural 4D perfusion values in HCC during TACE. The 3D spatial coverage of these intra-procedural perfusion maps enabled us to perform quantitative perfusion measurements of entire tumor volumes (in most cases). Whole tumor perfusion measurements should avoid irregularities associated with blood flow heterogeneity and 2D ROI selection, and should help improve the co-registration of measurements before and after administration of therapy. To date, there are few published values for quantitative clinical DCE-MRI perfusion measurements in HCC and only two prior studies have reported quantitative DCE-MRI perfusion measurements in rats with chemically-induced HCC (35) and in patients with metastatic liver tumors (28) respectively. Our pre-TACE TRIP-MRI HCC blood flow measurements of 16.3 (95% CI: 10.7–21.9) mL/min/100mL fell into the lower range of the mean hepatic arterial flow values measured in metastatic liver tumors during the prior study that included three metastasis patients (13.3, 27.1, 29.7 mL/min/100mL, respectively). However, our intra-procedural HCC perfusion measurements were much smaller than the previously reported mean hepatic arterial blood flow values of 94 or 32.7–201.9 mL/min/100mL in HCC (36,37) and 43–85 mL/min/100mL in metastatic liver tumors (36,38) measured using DCE-CT. These previous studies used either a dual-input single-compartment model, dual-input two-compartment DP model, or a peak gradient approach for data analysis, but all involved intravenous contrast medium injection with direct measurement of the AIF. The smaller values for our intra-procedural HCC perfusion measurements compared to those in previous intravenous based studies may have resulted from the following reasons: territorial assessment of single vessel blood supply proximal to the catheter tip excluded measurement of blood flow from any collateral arterial supply; local anesthesia during TACE may temporarily alter overall intra-procedural perfusion; catheter placement inside the hepatic arteries may possibly cause transient obstructions to arterial blood flow; the simplification of our analysis modeling approach, such as using a calculated rather than measured AIF and ignoring the bolus dispersion effects, may overestimate the contribution of the AIF; the effects of water exchange on quantitative CE MRI may lead to underestimation of perfusion, particularly while using our first-pass perfusion analysis approach; and whole tumor ROI selection inevitably included non-enhancing or necrotic tumor regions with little blood flow in our enrolled patient population, among whom many had tumors with sizes larger than 4 cm and/or had been previously treated with radiofrequency ablation or a prior chemoembolization. It is uncertain how these factors may influence the intra-procedural tumor perfusion measurement. Nevertheless, our intra-

procedural perfusion quantification should still offer a valuable “perfusion index” for monitoring catheter-directed embolotherapies (10,12,15).

Using quantitative 4D TRIP-MRI, we observed statistically significant differences in blood flow within the targeted tumors before and after TACE. We postulate that the intra-procedural reductions in our Fρ measurements are most likely related to the ischemic effects of the injected embolic material. The extent of intra-procedural perfusion changes specifically caused by the cytotoxic effects from injected chemotherapeutic agents remains undistinguishable. Furthermore, we observed a wide range of intra-procedural tumor perfusion reduction after TACE. Absolute perfusion reduction ranged from 0.1 to 60.0 (ml/min/100mL), percentage reductions ranged from 1% to 98%. This finding is consistent with previously reported semi-quantitative TRIP-MRI studies for monitoring TACE (12,17). This wide variability can be attributed to the currently employed subjective x-ray DSA embolic endpoint monitoring. Notably, a previous study by Lewandowski et al (10) found no correlation between SACE level and semi-quantitative MR perfusion reductions (only comparing measurements within central tumor slice).

Our study had several limitations. First, there lacks *in vivo* reference validation for this newly proposed quantitative 4D TRIP-MRI technique. Among possible reference validation methods, radiographic or fluorescence-labeled microsphere-based methods are not applicable for patient studies, intra-procedural CT would require additional patient transportation to a dedicated CT suite, and intra-procedural quantitative DCE-MRI with both intra-hepatic artery catheter placement and intravenous contrast injection for liver tumor perfusion, to our knowledge, has yet to be developed and validated. Second, quantitative 4D TRIP-MRI requires spatial co-registration among $B_1$, baseline $R_1$, and dynamic $R_1$ maps acquired at separate breath-holds. Image acquisition at exhalation position should help achieve a similar breath-hold position for each study. Future employment of motion correction and image co-registration algorithms should further alleviate this challenge. A previous breath-hold liver perfusion study reported reliable spatial co-registration between data collected on separate breath-holds after motion correction and image co-registration processing (39). Third, our first-pass perfusion analysis demands a high temporal resolution during TRIP-MRI volumetric sampling. We maintained our current temporal resolution at the expense of spatial resolution. Future improvements that increase temporal and spatial resolution should be sought. Fourth, whole tumor 4D TRIP-MRI perfusion measurements were effective for focal tumors with measurable margins, but can be difficult in diffuse infiltrative tumors with unclear borders. Fifth, the manual injection of contrast agent used in our study was less-than-ideal for the proposed AIF estimation using information about the bolus injection parameters. A power injector can be used to improve the precision and reproducibility of contrast injection. Sixth, the current tumor ROI selection was performed offline manually after TACE procedures. It would be desirable to define the tumor borders based upon online perfusion information, in order to assess effective tumor treatment intra-procedurally. Seventh, the limited number of hybrid x-ray DSA-MRI suite installations is a barrier to the widespread clinical application of intra-procedural MRI. It will take time for the new paradigm of functional MRI interventional guidance (40) to disseminate, and it will be imperative to prospectively assess how these MRI-guided interventional procedures can benefit patient care. Finally, we did not correlate intra-procudural 4D TRIP-MRI perfusion change with long-term clinical outcomes. In an ongoing study, we hope to address this topic with longitudinal clinical data and a larger patient sample size.

In conclusion, quantitative 4D TRIP-MRI can be performed successfully in an integrated x-ray DSA-MRI procedure suite to monitor intra-procedural reductions in liver tumor perfusion during TACE. This technique offers the ability to measure objective, quantitative changes in perfusion during therapy, and holds great promise to reveal important relationships between embolic endpoints and clinical outcomes after TACE. Such quantitative intra-procedural

perfusion changes may serve as a functional imaging biomarker to help optimize TACE in future clinical studies.

## References


1. El-Serag HB. Hepatocellular carcinoma: an epidemiologic view. J Clin Gastroenterol 2002;35:S72–78. [PubMed: 12394209]
2. Kew MC. Epidemiology of hepatocellular carcinoma. Toxicology 2002;181–182:35–38.
3. El-Serag HB, Davila JA, Petersen NJ, McGlynn KA. The continuing increase in the incidence of hepatocellular carcinoma in the United States: an update. Ann Intern Med 2003;139:817–823. [PubMed: 14623619]
4. Sato Y, Fujiwara K, Ogata I, et al. Transcatheter arterial embolization for hepatocellular carcinoma. Benefits and limitations for unresectable cases with liver cirrhosis evaluated by comparison with other conservative treatments. Cancer 1985;55:2822–2825. [PubMed: 2986826]
5. Llovet JM, Real MI, Montana X, et al. Arterial embolisation or chemoembolisation versus symptomatic treatment in patients with unresectable hepatocellular carcinoma: a randomised controlled trial. Lancet 2002;359:1734–1739. [PubMed: 12049862]
6. Charnsangavej C, Chuang VP, Wallace S, Soo CS, Bowers T. Angiographic classification of hepatic arterial collaterals. Radiology 1982;144:485–494. [PubMed: 6285413]
7. Soo CS, Chuang VP, Wallace S, Charnsangavej C, Carrasco H. Treatment of hepatic neoplasm through extrahepatic collaterals. Radiology 1983;147:45–49. [PubMed: 6828758]
8. Guo WJ, Li J, Chen Z, et al. Transient increased expression of VEGF and MMP-1 in a rat liver tumor model after hepatic arterial occlusion. Hepatogastroenterology 2004;51:381–386. [PubMed: 15086165]
9. Virmani S, Rhee TK, Ryu RK, et al. Comparison of hypoxia-inducible factor-1alpha expression before and after transcatheter arterial embolization in rabbit VX2 liver tumors. J Vasc Interv Radiol 2008;19:1483–1489. [PubMed: 18922400]
10. Lewandowski RJ, Wang D, Gehl J, et al. A comparison of chemoembolization endpoints using angiographic versus transcatheter intraarterial perfusion/MR imaging monitoring. J Vasc Interv Radiol 2007;18:1249–1257. [PubMed: 17911515]
11. Wilson MW, Kerlan RK Jr, Fidelman NA, et al. Hepatocellular carcinoma: regional therapy with a magnetic targeted carrier bound to doxorubicin in a dual MR imaging/conventional angiography suite--initial experience with four patients. Radiology 2004;230:287–293. [PubMed: 14695402]
12. Larson AC, Wang D, Atassi B, et al. Transcatheter intraarterial perfusion: MR monitoring of chemoembolization for hepatocellular carcinoma--feasibility of initial clinical translation. Radiology 2008;246:964–971. [PubMed: 18309018]
13. Larson AC, Rhee TK, Deng J, et al. Comparison between intravenous and intraarterial contrast injections for dynamic 3D MRI of liver tumors in the VX2 rabbit model. J Magn Reson Imaging 2006;24:242–247. [PubMed: 16758469]
14. Wang D, Bangash AK, Rhee TK, et al. Liver tumors: monitoring embolization in rabbits with VX2 tumors--transcatheter intraarterial first-pass perfusion MR imaging. Radiology 2007;245:130–139. [PubMed: 17885186]
15. Lewandowski RJ, Tepper J, Wang D, et al. MR imaging perfusion mismatch: a technique to verify successful targeting of liver tumors during transcatheter arterial chemoembolization. J Vasc Interv Radiol 2008;19:698–705. [PubMed: 18440458]
16. Virmani S, Wang D, Harris KR, et al. Comparison of transcatheter intraarterial perfusion MR imaging and fluorescent microsphere perfusion measurements during transcatheter arterial embolization of rabbit liver tumors. J Vasc Interv Radiol 2007;18:1280–1286. [PubMed: 17911519]
17. Gaba RC, Wang D, Lewandowski RJ, et al. Four-dimensional transcatheter intraarterial perfusion MR imaging for monitoring chemoembolization of hepatocellular carcinoma: preliminary results. J Vasc Interv Radiol 2008;19:1589–1595. [PubMed: 18818097]
18. Wang D, Virmani S, Tang R, et al. Four-dimensional transcatheter intraarterial perfusion (TRIP)-MRI for monitoring liver tumor embolization in VX2 rabbits. Magn Reson Med 2008;60:970–975. [PubMed: 18816818]

19. Brown DB, Cardella JF, Sacks D, et al. Quality improvement guidelines for transhepatic arterial chemoembolization, embolization, and chemotherapeutic infusion for hepatic malignancy. J Vasc Interv Radiol 2006;17:225–232. [PubMed: 16517768]
20. Georgiades CS, Hong K, D'Angelo M, Geschwind JF. Safety and efficacy of transarterial chemoembolization in patients with unresectable hepatocellular carcinoma and portal vein thrombosis. J Vasc Interv Radiol 2005;16:1653–1659. [PubMed: 16371532]
21. Bruix J, Sherman M, Llovet JM, et al. Clinical management of hepatocellular carcinoma. Conclusions of the Barcelona-2000 EASL conference. European Association for the Study of the Liver. J Hepatol 2001;35:421–430. [PubMed: 11592607]
22. Soresi M, Magliarisi C, Campagna P, et al. Usefulness of alpha-fetoprotein in the diagnosis of hepatocellular carcinoma. Anticancer Res 2003;23:1747–1753. [PubMed: 12820452]
23. Wang D, Zuehlsdorff S, Larson AC. Rapid 3D radiofrequency field mapping using catalyzed double-angle method. NMR Biomed 2009;22:882–890. [PubMed: 19492303]
24. Wang, D.; Zuehlsdorff, S.; Omary, RA.; Larson, AC. Targeted B1+ Mapping using 3D Reduced Field-of-View Catalyzed Double-Angle Method. Proceedings of the 17th Annual Meeting of ISMRM; Honolulu, Hawaii, USA. 2009. (Abstract 370)
25. Pintaske J, Martirosian P, Graf H, et al. Relaxivity of Gadopentetate Dimeglumine (Magnevist), Gadobutrol (Gadovist), and Gadobenate Dimeglumine (MultiHance) in human blood plasma at 0.2, 1.5, and 3 Tesla. Invest Radiol 2006;41:213–221. [PubMed: 16481903]
26. Donahue KM, Weisskoff RM, Burstein D. Water diffusion and exchange as they influence contrast enhancement. J Magn Reson Imaging 1997;7:102–110. [PubMed: 9039599]
27. Judd RM, Reeder SB, May-Newman K. Effects of water exchange on the measurement of myocardial perfusion using paramagnetic contrast agents. Magn Reson Med 1999;41:334–342. [PubMed: 10080282]
28. Koh TS, Thng CH, Lee PS, et al. Hepatic metastases: in vivo assessment of perfusion parameters at dynamic contrast-enhanced MR imaging with dual-input two-compartment tracer kinetics model. Radiology 2008;249:307–320. [PubMed: 18695207]
29. St Lawrence KS, Lee TY. An adiabatic approximation to the tissue homogeneity model for water exchange in the brain: I. Theoretical derivation. J Cereb Blood Flow Metab 1998;18:1365–1377. [PubMed: 9850149]
30. Tofts PS, Brix G, Buckley DL, et al. Estimating kinetic parameters from dynamic contrast-enhanced T(1)-weighted MRI of a diffusable tracer: standardized quantities and symbols. J Magn Reson Imaging 1999;10:223–232. [PubMed: 10508281]
31. Annet L, Materne R, Danse E, Jamart J, Horsmans Y, Van Beers BE. Hepatic flow parameters measured with MR imaging and Doppler US: correlations with degree of cirrhosis and portal hypertension. Radiology 2003;229:409–414. [PubMed: 12970464]
32. Van Beers BE, Leconte I, Materne R, Smith AM, Jamart J, Horsmans Y. Hepatic perfusion parameters in chronic liver disease: dynamic CT measurements correlated with disease severity. AJR Am J Roentgenol 2001;176:667–673. [PubMed: 11222202]
33. Hendee WR. Special report: biomedical imaging research opportunities workshop IV--a summary of findings and recommendations. Radiology 2007;242:338–341. [PubMed: 17255405]
34. Buckley DL. Uncertainty in the analysis of tracer kinetics using dynamic contrast-enhanced T1-weighted MRI. Magn Reson Med 2002;47:601–606. [PubMed: 11870848]
35. Michoux N, Huwart L, Abarca-Quinones J, et al. Transvascular and interstitial transport in rat hepatocellular carcinomas: dynamic contrast-enhanced MRI assessment with low- and high-molecular weight agents. J Magn Reson Imaging 2008;28:906–914. [PubMed: 18821616]
36. Tsushima Y, Funabasama S, Aoki J, Sanada S, Endo K. Quantitative perfusion map of malignant liver tumors, created from dynamic computed tomography data. Acad Radiol 2004;11:215–223. [PubMed: 14974597]
37. Chen G, Ma DQ, He W, Zhang BF, Zhao LQ. Computed tomography perfusion in evaluating the therapeutic effect of transarterial chemoembolization for hepatocellular carcinoma. World J Gastroenterol 2008;14:5738–5743. [PubMed: 18837093]
38. Blomley MJ, Coulden R, Dawson P, et al. Liver perfusion studied with ultrafast CT. J Comput Assist Tomogr 1995;19:424–433. [PubMed: 7790553]

39. Jackson A, Haroon H, Zhu XP, Li KL, Thacker NA, Jayson G. Breath-hold perfusion and permeability mapping of hepatic malignancies using magnetic resonance imaging and a first-pass leakage profile model. NMR Biomed 2002;15:164–173. [PubMed: 11870912]

40. Assumpcao L, Choti M, Pawlik TM, Gecshwind JF, Kamel IR. Functional MR imaging as a new paradigm for image guidance. Abdom Imaging 2009;34:675–685. [PubMed: 19048335]

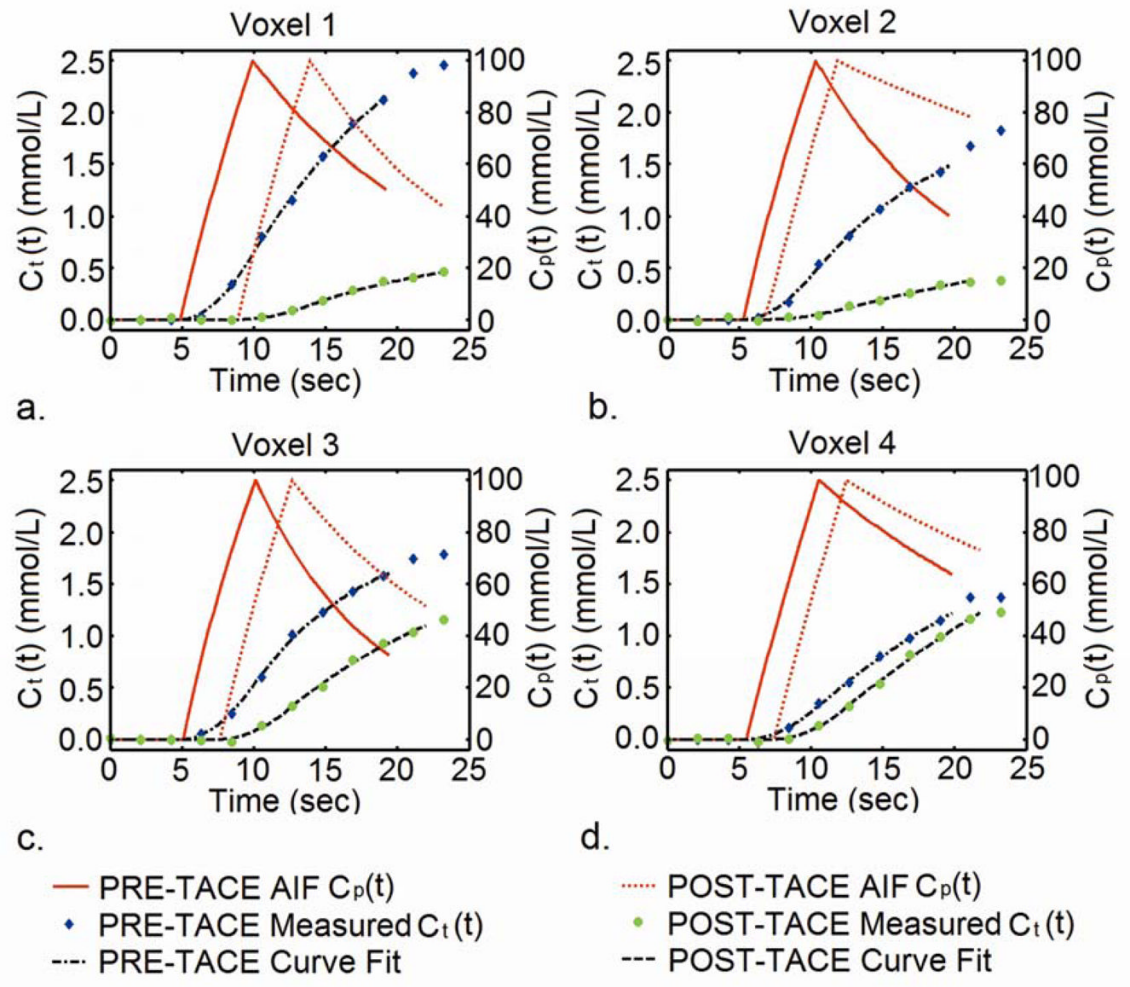


**Figure 1.**

Graphs show the measured $C_t(t)$ curves, estimated AIFs ($C_p(t)$), and associated interpolated curve fitting using proposed first-pass perfusion model for individual tumor voxels from one representative patient before and after TACE. The measured $C_t(t)$ curves clearly exhibited alteration in contrast uptake kinetics due to TACE.

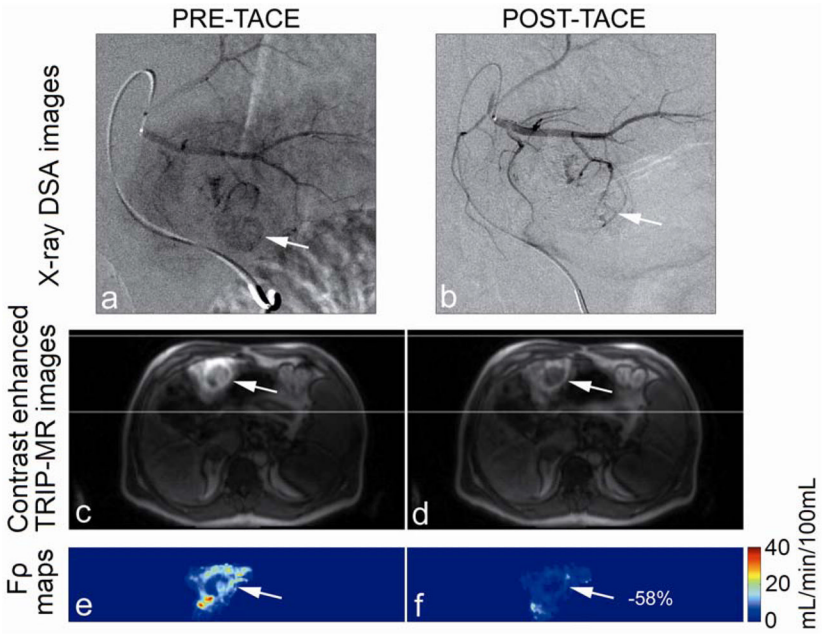


**Figure 2.**

Representative x-ray DSA-MRI monitored TACE images obtained in a 51-year-old patient with segment III HCC. X-ray DSA image before TACE (a) demonstrates catheter positioning, arterial structure, normal antegrade blood flow, and tumor blush (arrow). Post-TACE x-ray DSA image (b) demonstrates reduced antegrade blood flow and no tumor blush. Axial pre-TACE 4D TRIP-MR image after intraarterial contrast injection at peak enhancement (c) shows segmental liver enhancement and tumor position (arrows), and post-TACE peak enhanced 4D TRIP-MR image (d) shows reduced tumor contrast uptake; corresponding intra-procedural pre-TACE Fρ map (e) indicates baseline blood flow and post-TACE Fρ map (f) indicates reduced blood flow, in the tumor within the targeted vascular territories. The percentage perfusion reduction is listed in the post-TACE perfusion map.

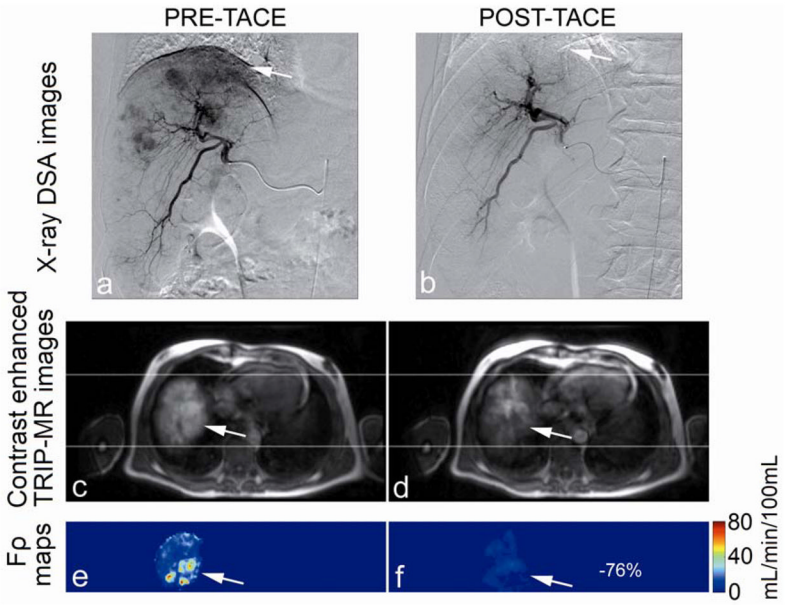


**Figure 3.**

Representative x-ray DSA-MRI monitored TACE images obtained in a 55-year-old patient with right lobe HCC. X-ray DSA image before TACE (a) demonstrates catheter positioning, arterial structure, normal antegrade blood flow, and tumor blush (arrow). Post-TACE x-ray DSA image (b) demonstrates reduced antegrade blood flow and disappearing tumor blush. Axial pre-TACE 4D TRIP-MR image after intraarterial contrast injection at peak enhancement (c) shows lobar liver enhancement and tumor position (arrows), and post-TACE peak enhanced 4D TRIP-MR image (d) shows reduced tumor contrast uptake; corresponding intra-procedural pre-TACE Fρ map (e) indicates baseline blood flow and post-TACE Fρ map (f) indicates reduced blood flow, in the tumor within the targeted vascular territories. The percentage perfusion reduction is listed in the post-TACE perfusion map.

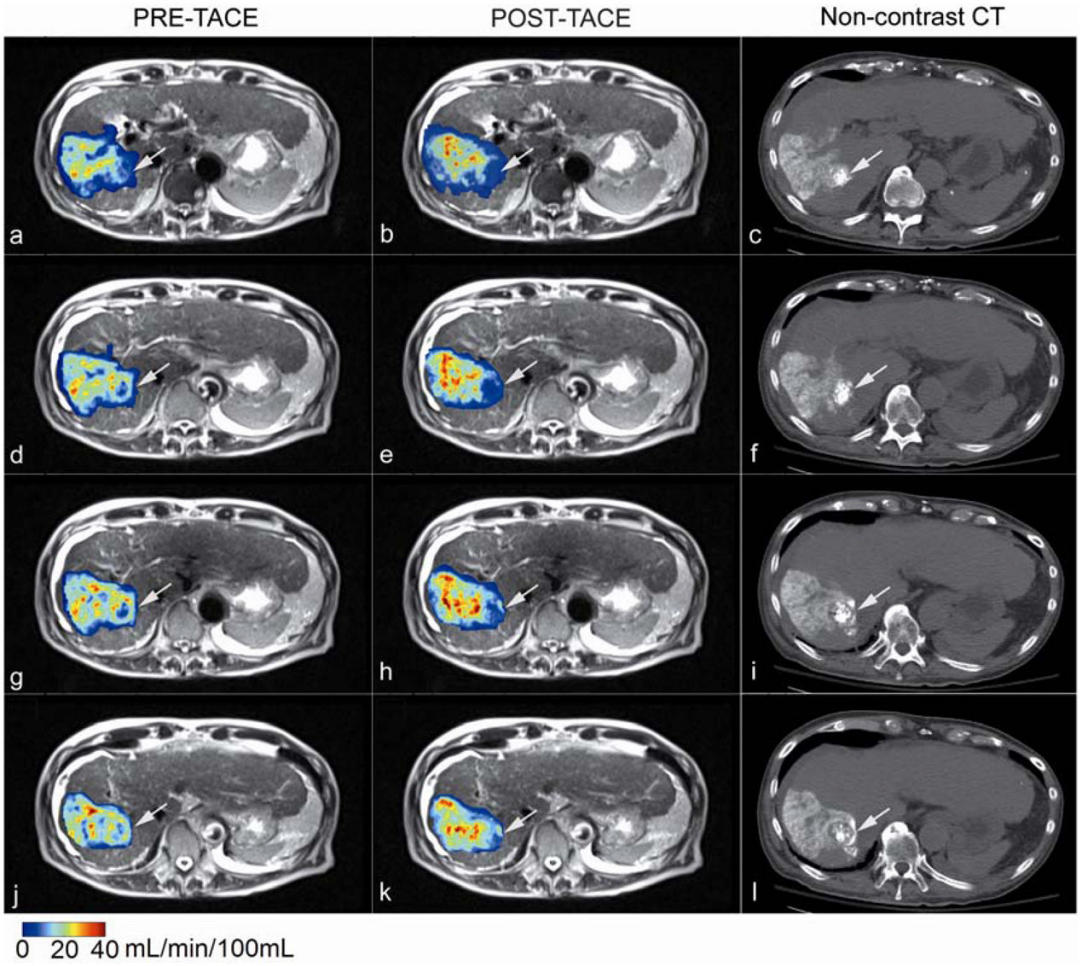


**Figure 4.**

Intra-procedural 4D perfusion maps with anatomic MR images, and post-TACE CT images at four adjacent slice positions obtained in an 81-year-old patient with segment VII HCC. Quantitative Fρ maps fused with axial T2-weighted anatomic images acquired during x-ray DSA-MRI monitored TACE (a, b, d, e, g, h, j, k) spatially reveal TACE-induced perfusion reductions in the targeted tumor (arrows). Non-contrast enhanced axial CT images obtained immediately after TACE (c, f, i, l) qualitatively verify chemotherapy emulsion distribution, showing ethiodized oil contrast accumulation in the regions of perfusion reduction in the targeted tumor (arrows).

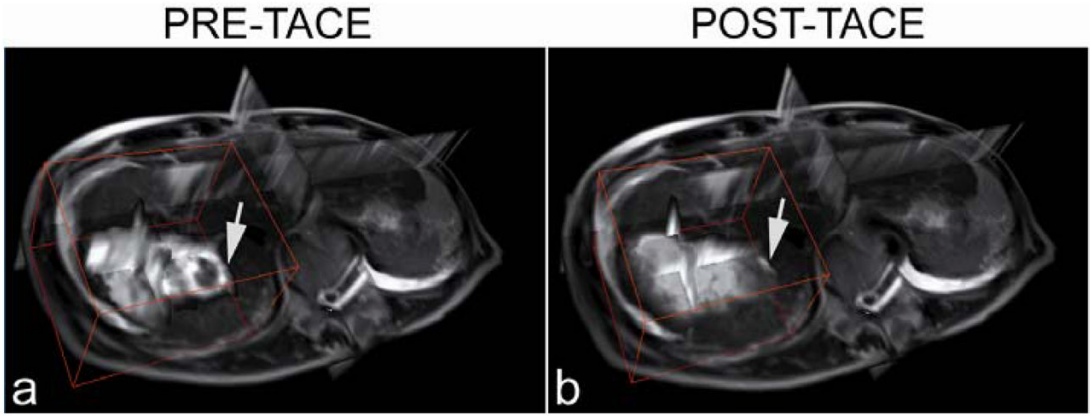


**Figure 5.**
Quantitative 4D intra-procedural Fρ maps co-registered to T2-weighted anatomic images acquired during x-ray DSA-MRI monitored TACE in an 81-year-old patient with segment VII HCC. These Fρ maps provide localized intra-procedural perfusion information with volumetric coverage within the targeted treatment region. Arrows indicate tumor position.

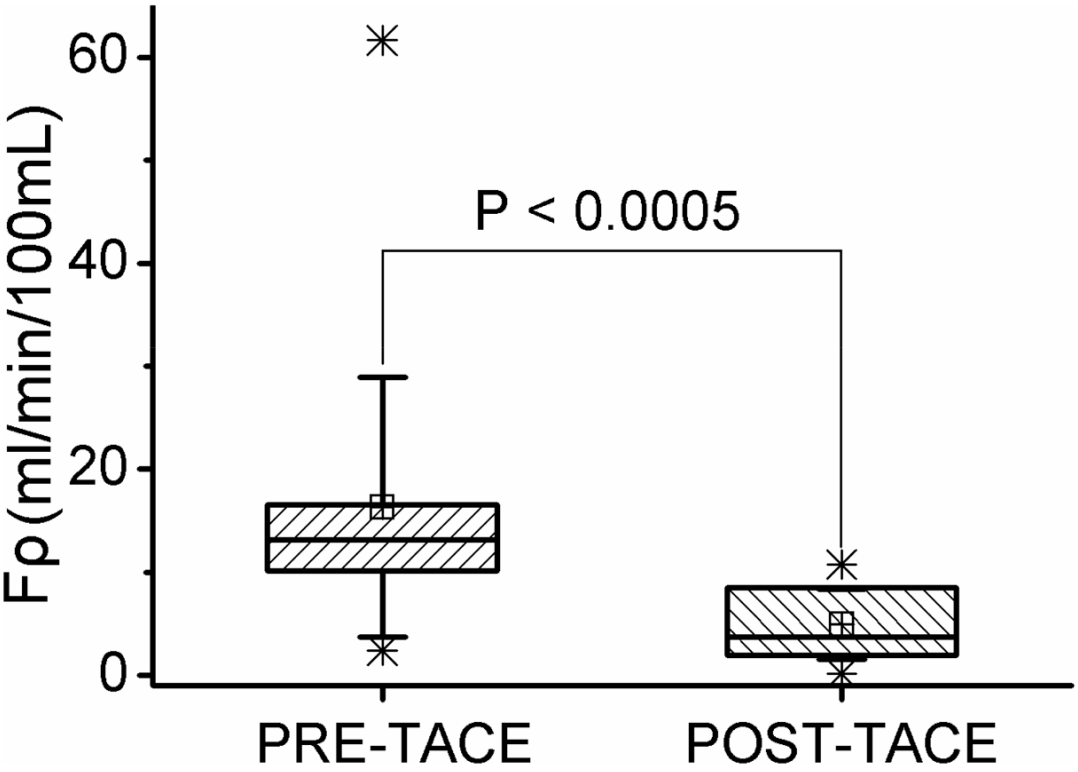


**Figure 6.**
Box plot show the distribution of intra-procedural tumor perfusion and a statistically significant tumor Fρ reduction after TACE. Boxes represent the lower and upper quartiles; line inside each box labels the 50th percentile (median); small crossed squares show the mean value; whiskers indicate the standard deviation; Stars (*) represent one and ninety-nine percentiles.

## Table 1

Patient and Tumor Characteristics

| | |
|---|---|
| **Gender** | |
| Male | 12 (75) |
| Female | 4 (25) |
| **Age** | |
| Average ± SD (y) | 63 ± 9 |
| **Lesion Distribution** | |
| Unilobar | 9 (56) |
| Bilobar | 7 (44) |
| **Maximum Diameter of Largest Target Lesion** | |
| Average ± SD (cm) | 4.5 ± 3.4 |
| <4 | 9 (56) |
| ≥4 | 7 (44) |
| **Replacement (%)** | |
| <25 | 15 (94) |
| 25–50 | 0 (0) |
| >50 | 1 (6) |
| **Morphology** | |
| Unifocal | 8 (50) |
| Multifocal | 8 (50) |
| **Portal Vein Thrombosis** | |
| None | 13 (81) |
| Unilobar | 3 (19) |
| Bilobar | 0 (0) |
| **Cirrhosis** | |
| No | 1 (6) |
| Yes | 15 (94) |

Note.—Values in parentheses are percentages.